JCTC Journal of Chemical Theory and Computation

Toward a Coarse Graining/All Atoms Force Field (CG/AA) from a Multiscale Optimization Method: An Application to the MCM-41 Mesoporous Silicates

A. Ghoufi,*,† D. Morineau,† R. Lefort,† and P. Malfreyt‡

Institut de Physique de Rennes, UMR 6251 CNRS, Université de Rennes 1, France

Thermodynamique et Interactions Moléculaires, UMR CNRS 6272, Université Blaise Pascal, France

Received March 29, 2010

Abstract: Many interesting physical phenomena occur on length and time scales that are not accessible by atomistic molecular simulations. By introducing a coarse graining of the degrees of freedom, coarse-grained (CG) models allow ther study of larger scale systems for longer times. Coarse-grained force fields have been mostly derived for large molecules, including polymeric materials and proteins. By contrast, there exist no satisfactory CG potentials for mesostructured porous solid materials in the literature. This issue has become critical among a growing number of studies on confinement effects on fluid properties, which require both long time and large scale simulations and the conservation of a sufficient level of atomistic description to account for interfacial phenomena. In this paper, we present a general multiscale procedure to derive a hybrid coarse grained/all atoms force field CG/AA model for mesoporous systems. The method is applied to mesostructured MCM-41 molecular sieves, while the parameters of the mesoscopic interaction potentials are obtained and validated from the computation of the adsorption isotherm of methanol by grand canonical molecular dynamic simulation.

1. Introduction

Considerable effort has been devoted to the study of molecular fluids confined in mesoporous/nanoporous solids.[1−4] Confined systems exhibit very original features, in terms of structural arrangements, molecular dynamics, and phase transitions (freezing, melting, capillary condensation, and mesomorphic transitions), which cannot be simply understood from the properties of the bulk system.[5−10] According to the abundant literature on the matter, it has been recognized that the properties of confined systems are not simply related to the typical size of the confining medium but are intimately related to the details of the porous morphology and the structure and chemistry of the pore surface.[11−15] This significantly complicates the interpretation of experimental results and their comparison with theoretical predictions based on simple pore models (structureless pore, simple geometry). Molecular simulations of fluids adsorbed in realistic pores offer unique possibilities to connect some macroscopic properties to a microscopic description of the physical phenomena at play in nanoconfined phases. As a result, molecular simulations have become widespread in the literature and have become a powerful method to investigate mesoporous confinement effects.[1,4] Fully atomistic simulations, which allow a realistic account of the details of the confining medium and the surface interaction, are also very time-consuming. This usually becomes a serious drawback to investigating long-time adsorption and relaxation processes, which are usual in confined systems as well as those with large pore sizes (e.g., 10 nm and more). To overcome these difficulties, coarse-grained force fields CG[16] and mesoscopic methods—such as dissipative particules dynamics[17,18]—have been designed for biological[19] and polymeric systems.[20] Much benefit could be gained from the development of mesoscopic methods for porous solid materials,

* Corresponding author e-mail: aziz.ghoufi@univ-rennes1.fr.
† Université de Rennes 1.
‡ Université Blaise Pascal.

10.1021/ct100169r
Published on Web 09/14/2010

which surprisingly have not been given full attention.[21] A realistic CG potential for mesoporous solids should necessarily incorporate a part of modeling at the atomistic level in order to describe the specific interfacial interactions, which play a fundamental role in confinement phenomena. The situation shares some similarities with the question of folding proteins, which has been treated with hybrid potential models.[16,22] However, the approaches derived in the latter case cannot be simply transferred to the case of solid systems. Another approach proposed by Dupuis et al.[21] extends the quasi-continuum method to treat the dynamics of crystalline solids at a constant temperature. This method is based upon the calculation of the potential of mean force. Its accuracy is determined by the sampling of the solid atoms' positions in the molecular dynamics (MD) simulations. This method is not designed for the determination of the CG potential for porous solids, which are generally approximated as rigid systems in numerical studies of adsorption. Alternatively, Dubbeldam et al.[23] used an iterative search for Lennard-Jones parameters to reproduce the inflection points in isotherms of adsorption. This full microscopic method does not allow one to obtain the intrinsic parameters of porous solids because we only obtain the crossed (framework/adsorbate) interactions parameters. Then, the obtained parameters are not transferable, and the method must be applied for each adsorbate.

In the present paper, we introduce a hybrid coarse grained/all atoms force field CG/AA for porous materials. We detail a general procedure to determine the mesoscopic potential parameters using a multiscale method based on the computation of the isotherm of adsorption by molecular simulations. The method proposed here is developed in close connection with atomistic models, but it is based upon a very different approach from iterative Boltzman inversion,[24] inverted Monte Carlo schemes,[25,26] or force matching methods.[27] Recently, Das and Andersen[28] used a force matching method based on a multiscale approach and the computation of the potential of mean force for solutes. They propose new basis functions for the variational calculation. This method is quite accurate, provided that the phase space is correctly sampled, but the grid potential does not provide a general force field. Here, we present a coarse grained force field resulting from an optimization procedure of energetic parameters to model the porous solid. This method is based on the calculation and optimization of the macroscopic properties, allowing one to provide the intrinsic parameters of porous material. Our CG/AA force field can be easily combined with the CG or AA solvent/adsorbat. Besides, we do not need to compute the grid of potential as it is done in the force matching approach.[28] The goal of our study is to provide a simple method that can be used to derive computationally fast and practical models of porous solids. Thereby, we report a CG/AA force field for MCM-41 types of mesoporous silicates modeled by SiO_4 and SiO_3OH units, the interaction parameters of which are obtained from the isotherm of adsorption of methanol. Already, there exist some simplifications to decrease the computational time as the rigid consideration. However, at variance with the usual AA rigid framework model (decreasing of the intramolecular of degree of freedom), our CG/AA rigid description allows one to decrease the number of centers of force.

We opt for a highly hydrated MCM-41 because it is one of the most studied forms of silicate used in molecular simulations, and thus it can be considered as a reference system. This system is especially suited for a validation of our method by comparing some adsorption and dynamic properties between the AA and the CG/AA models. In addition, we apply our method for another MCM-41 with a lower hydratation level, which provides a more realistic description of some experimental porous materials. The improvement provided by this approach allows the simulation of large scale mesoporous systems while keeping the possibility of later tuning the nature of the surface interaction, which is a currently debated issue in a number of experimental studies. The properties of confined methanol have already been addressed in numerical and experimental studies.[29−33] They have provided us with useful groundwork for the development and the validation of the CG/AA force field. The first milestone of this study stands on the methodological side and consists of the validation of the coarse-graining approach, by comparing adsorption and dynamics results between the AA and the CG/AA models.

2. The Simulation Models

2.1. The Atomistic Model. *Highly Hydrated (HH) MCM-41: $\rho_{OH} = 7.5$ OH/nm^2.* Simulations of confined methanol have been performed by building a realistic model of the porous silicate used experimentally. This is required to account for the complexity of the liquid−substrate interactions and confinement effects. Since the geometry of the porous MCM-41 is properly characterized in terms of channels of a definite section, it has been possible to produce comparable conditions of confinement. We derived an atomic description of the silicate starting from an equilibrium structure of amorphous silica within a cubic cell of 36 Å on a side provided by Vink and Barkema.[34] Then, we applied a procedure proposed by Brodka and Zerda[35] to consider a realistic porosity within the amorphous silica. We first generate a cavity along the z axis of the silica cell by removing the atoms within a cylinder of diameter (D) 24 Å. From their coordination numbers, we distinguished bridging oxygens (O_b) bonded to two silicon atoms from nonbridging oxygens (O_{nb}) bonded to only one silicon and bonded to one hydrogen atom (H_{nb}). An iterative procedure of atom (O and Si) removal was applied until only tetra-coordinated silicon atoms, bonded to a maximum of two O_{nb}'s, were present in the structure. Finally, nonbridging oxygens were saturated with hydrogen atoms to form surface hydroxyl groups. Although the silica matrix was subsequently kept rigid, rotation around the Si−O bond of the hydroxyl groups was allowed. In the MC procedure, we used a trial rotation move of the H atom around the Si−O bond. The parameters of the bending potential ($U_\theta = k_\theta(\theta - \theta_0)^2$) are $k_\theta = 284.37$ kJ mol^{-1} rad^{-2} and $\theta_0 = 118°$ where k_θ is the constant of force and θ_0 the equilibrium angle. This procedure leads to a realistic description of the irregular inner surface of the porous silicate and of the interfacial interactions between

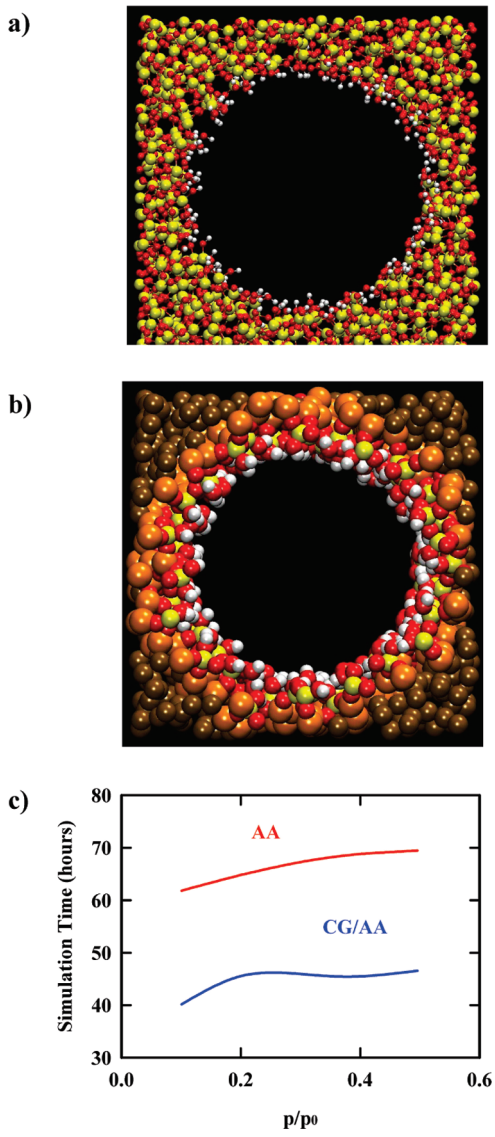

Figure 1. AA (a) and CG/AA (b) description of MCM-41. Red indicates the oxygen atoms. The hydrogen positions are in white. Yellow are the silicon atoms, orange the SiO_{4-x} CG beads, and brown the SiO_4 CG beads. (c) Times of simulation for both models as a function of the reduced pressure. The simulations were performed using a time step of 0.002 ps to sample 2 ns, e.g., 10^6 MD steps.

the fluid and the matrix. The inner surface coverage of silanol groups was about 7.5 per square-nanometer, which is comparable to previous models of surface silica and correspond to highly hydrated actual silica (HH MCM-41).[12,35] The resulting pore morphology is shown in the snaphots in Figure 1a.

For AA and CG/AA models, the total intermolecular potential is a sum of the electrostatic and Lennard-Jones interactions (eq 1).

$$U = \sum_{i}^{N-1} \sum_{a}^{n_i} \sum_{j=i+1}^{N} \sum_{b}^{n_j} \left[\frac{q_a q_b}{4\pi\varepsilon_o r_{iajb}} + 4\varepsilon_{ab} \left(\left(\frac{\sigma_{ab}}{r_{iajb}} \right)^{12} - \left(\frac{\sigma_{ab}}{r_{iajb}} \right)^{6} \right) \right] \quad (1)$$

In eq 1, q_i is the charge of the i atom, ε_{ab} and σ_{ab} are the different Lennard-Jones parameters calculated from Lorentz−Berthelot mixing rules ($\sigma_{ab} = (\sigma_{aa} + \sigma_{bb})/2$, $\varepsilon_{ab} = \sqrt{(\varepsilon_{aa}\varepsilon_{bb})}$). Note that Lorentz−Berthelot mixing rules have been also applied for the CG model. r_{iajb} is the distance between atom a of molecule i and b of j. n_i is the number of particles in the i group. We consider the adsorption of CH_3OH in the gas phase for its simplicity. To model CH_3OH, we used the TRAPPE force field developed by Siepmann et al.[36] (Table 1), which was validated on the liquid−vapor diagram of phase.

Table 1. Force Field Parameters of MCM-41 Resulting from the Optimization Procedure[a]

	σ (Å)	ε (kJ mol^{-1})	q(u.e)
		MCM-41	
		AA Force Field	
H_{nb}	0.000	0.000	0.206
O_b	2.700	1.912	−0.6349
O_{nb}	3.000	1.912	−0. 5399
Si	0.000	0.000	1.2739
		CG/AA Force Field	
H_{nb}	0.000	0.000	0.206
O_b	2.700	1.622	−0.6349
O_{nb}	2.700	1.622	−0.5399
Si	0.000	0.000	1.2739
SiO_3	4.500	0.832	0.950
SiO_2	4.500	0.832	0.638
SiO	4.500	0.832	0.320
SiO_4	5.500	2.411	0.0054
		CH_3OH	
CH_3	3.750	0.815	0.265
O_H	3.020	0.773	−0.700
H_O	0.000	0.000	0.435

[a] For SiO_{4-x}, the charge depends on the number x of oxygen atoms of the silicon's first coordination shell that are modelled by the (AA) description. The geometric characteristics of methanol are given in Ref. 36.

Weakly Hydrated (WH) MCM-41: $\rho_{OH} = 3.4$ OH/nm^2. A porous framework with a lower density of silanol groups ($\rho_{OH} = 3.4$/nm^2), lately denoted as the weakly hydrated (WH) MCM-41, was built using the HH MCM-41 as a starting structure. Dehydration of the pore surface was obtained by removing the OH group and the oxygen atom engaged together in a hydrogen bond between randomly selected couples of adjacent silanol groups. An explicit chemical bound was then created so that the remaining oxygen bridges the two surface silicon atoms considered. We repeated this iterative procedure until the targeted surface density of the silanols groups was achieved. The obtained structure was allowed to relax during MD simulations of duration $t = 5$ ns, with a harmonic description of the Si−O bond ($U = k_0(r - r_0)^2$) with an equilibrium distance $r_0 = 1.58$ Å and a force constant $k_0 = 2000$ kJ mol^{-1}. The total residual charge introduced by this dehydration process (+1.1 u.e.) has been homogeneously redistributed over the interaction sites of the system. It corresponds to a tiny increase by $\delta q \sim 0.0001$ u.e. of the charge assigned to each electrostatic site.

The resulting WH porous structure presents a less hydrophilic character with respect to the HH MCM-41. The radial density profiles of the two types of empty MCM-41 (cf. Figure 2a) agree with a comparable average value of the pore radius of about 12 Å. Direct insight into the inner pore

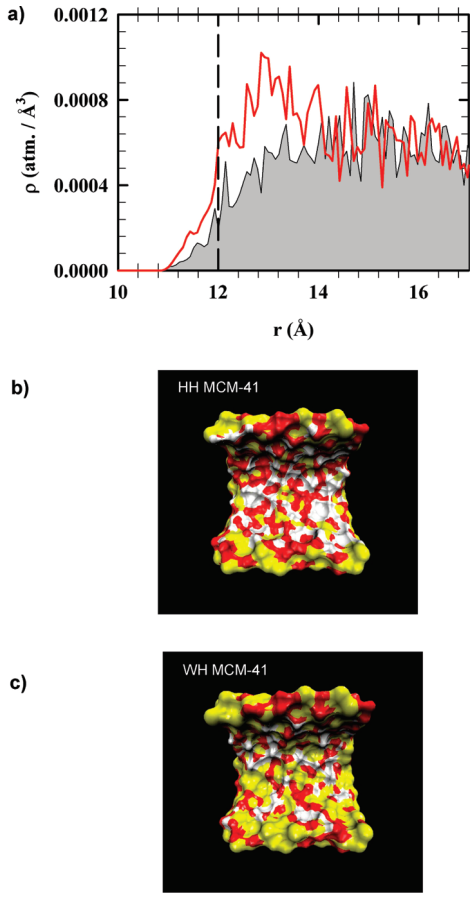

Figure 2. (a) Radial density profile of MCM-41 for HH (red) and WH (gray zone) types of MCM-41. Connolly's surface of HH (b) and WH (c) MCM-41. Red, white, and yellow colors indicate the oxygen, hydrogen, and silicon atoms, respectively.

surface coverage of the two types of materials is provided from the surface Connolly diagrams displayed in Figure 2b and c.

2.2. Derivation of the Coarse-Grained Force Field. SiO_3OH silanol groups located on the internal pore surface confer a hydrophilic character to the hydrated porous silicates and can promote the formation of hydrogen bonds (Hb) with associating fluids, which strongly affect the structural organization and the dynamics of the adsorbates. Interfacial hydrogen bonds and hydrophilic interactions are some fundamental aspects of the physics of confined phases. Hence, silanol groups must be considered as a foremost ingredient of any reliable force field which aims at modeling porous silicates. The multiscale coarse-graining strategy that we have adopted provides a hybrid force field where the surface atoms and the hydrogen bonds are described at the atomistic level, whereas a coarse-grained description is used for the groups of atoms far away from the internal surface. To define the CG beads, we decompose the framework in three parts according to a layered description depicted in Figure 1b. The CG appellation is preferred to the one of united atoms (UA) because this force field does not include explicit representation of nonpolar hydrogen atoms and only polar hydrogens are included in the force field definition. Additionally, our description is in line with the CG statistical physics. The first layer (N_1) corresponds to the silanol SiO_3OH groups treated with an atomistic description. In this atomistic description, distinction is made between bridging oxygens (O_b), which are bonded to two silicon atoms and nonbridging oxygens (O_{nb}) bonded to only one silicon and one silanol hydrogen atom. The second layer (N_2) corresponds to the nonsilanol groups bonded to $x = 1$, 2, or 3 oxygen atoms of N_1 and which were treated as CG beads, denoted SiO_{4-x}. In this case, one bead stands for a coarse-grained description of the force field, which corresponds to one silicon atom and half the interaction of the $4 - x$ bridging oxygens in the atomistic model. Different values of the force field parameters are obtained depending on the coordination number x, as explained later. The second type of CG bead, denoted N_3, is introduced for the remaining SiO_4 groups, which are connected to N_2 and/or N_3 beads. In the latter case, the bead stands for the atomistic interaction arising from one silicon atom and half the interaction arising from the oxygens within the 4-fold coordination shell. Figure 1b shows a picture of this arrangement. According to this description, the surface is covered by −SiOH and Si−O−Si to get a physical picture of the atomistic description. As the electrostatic field is independent of the description level, the mesoscopic charge of each bead is the sum of the AA charges of atoms participating in one CG particle. Nevertheless, one should pay great attention to the definition of the CG charges of SiO_{4-x} beads, which make the link between the coarse-grained and atomistic parts of the sample. According to the definition, the silicon atom of a SiO_{4-x} bead is connected to $x = 1$, 2, or 3 oxygens, which is/are explicitly treated by an atomistic AA force field. Therefore, the net mesoscopic charge reflecting the silicon and half the interaction from the oxygens not treated by the AA model is $q_{Si}^{AA} + (4 - x)/(2)q_O^{AA}$. The calculation of q_{SiO_4} is deduced by dividing the residual charge by the total number of silicons in the layer (N_3) so as to satisfy electric charge neutrality. The charges of the different sites of the coarse-grained model are summarized in Table 1. We opt for the simplest degree of coarse-grained (1 CG unit = SiO_x ($x = 1, 4$)). However, it is possible to undertake a study using an higher degree of CG, but our main point was to test and validate our multiscale optimization.

Once the CG beads are defined, we opt as a center of force the center of mass of each CG unit. The Lennard-Jones parameters (σ^{CG} and ε^{CG}) have been obtained and refined from the simulation of the isotherm of adsorption of methanol at $T = 300$ K, the results of which are detailed in the next section. Adsorption quantities have been calculated from the simulations of the CG and AA models and have been used as inputs in the merit function (F; eq 2). The parameters of the CG model have been optimized by minimization of the value of F according to a procedure discussed in ref 37.

$$F = \frac{1}{n}\sum_{i=1}^{n}\frac{[f_i^{CG/AA} - f_i^{AA}]}{s_i^2} \qquad (2)$$

In eq 2, s_i is the estimated statistical uncertainty and $s_i^2 = (s_i^{CG/AA})^2 + (s_i^{AA})^2$, f_i^{AA}, and $f_i^{CG/AA}$are the values of the ith physical property on n, which were calculated by simulation of the AA and CG/AA models, respectively. In the present

case, $n = 2$, and the two properties considered were the enthalpy of adsorption $\Delta_r H_{ads}$ and the adsorbed amount n_{ads}. The Lennard-Jones parameters have been optimized for SiO_{4-x}, SiO_4, O_b, O_{nb}, and H_{nb}, whereas they are identical to the all atoms force field for the silicon atoms. The choice to keep the AA parameters for silicon atoms in the coarse-grained description of silica has been justified by the fact that they do not vary significantly if they are considered as free parameters in the refinement procedure (about 0.2% change). This is most probably a consequence of the distant location of Si from the inner surface with regard to other species (H_b, O_b, and O_{nb}), which reduce their influence on the diffusion and adsorption processes. The minimum condition of F is that every partial derivative must be zero, which means solving eq 3. Equation 3 is a function of $(\partial f_i^{CG/AA})/(\partial y_k)$ where y_k is one of the p different optimized potential parameters.

$$\sum_{i=1}^{n}\left[\frac{f_i^{CG/AA}(y_j^o) - f_i^{AA} + \sum_{k=1}^{p}\frac{\partial f_i^{CG/AA}}{\partial y_k}\Delta y_k}{s_i^2}\right]\frac{\partial f_i^{CG/AA}}{\partial y_j} = 0, \quad j = 1, ..., p \tag{3}$$

$\Delta y_k = y_k - y_k^o$ is the difference between the refined value y_k and the initial value y_k^o of the kth potential parameter. In our study, $n = 2$ and $p = 10$. The partial derivates $(\partial f_i^{CG/AA})/(\partial y^k)$ are calculated using the fluctuation relation[38] as indicated in relation 4.

$$\frac{\partial\langle X\rangle}{\partial y_k} = \left\langle\frac{\partial X}{\partial y_k}\right\rangle - \beta\left(\left\langle X\frac{\partial U}{\partial y_k} - \langle X\rangle\left\langle\frac{\partial U}{\partial y_k}\right\rangle\right\rangle\right) \tag{4}$$

$\langle ... \rangle$ indicates the ensemble average in the canonical statistical ensemble. We give the final expression of $(\partial\langle\Delta_r H_{ads}\rangle)/(\partial y_k)$ and $(\partial\langle n_{ads}\rangle)/(\partial y_k)$ in the appendix. The result of our optimization is given in Table 1. For Lennard-Jones parameters, we provide the intrinsic terms (aa) while the crossed terms (ab) are calculated using the Lorentz−Berthelot combining rules ($\sigma_{ab}^{CG} = (\sigma_{aa}^{CG} + \sigma_{bb}^{CG})/2$; $\varepsilon_{ab}^{CG} = \sqrt{(\varepsilon_{aa}^{CG}\varepsilon_{bb}^{CG})}$). Smaller values of σ (i.e., more attractive) were obtained for the O_{nb} and O_b parameters with respect to the AA description. This can be attributed to some changes in the local environment interaction, which effectively counterbalance the highly repulsive contribution of the mesoscopic beads. For the Lennard-Jones (LJ) parameters, different initial values were used to account for the microscopic difference between each unit. The optimized final values are very close to each other, indicating a weak dispersive/repulsive interaction between the adsorbant and the framework, which can be safely averaged over the atoms constituting each unit.

First, we applied the same procedure to derive the CG/AA model corresponding to the WH type of MCM-41 from the WH AA framework. Moreover, a CG/AA model of the WH type of MCM-41 was obtained after dehydration and thermal relaxation of the HH CG/AA matrix, following the procedure described in section 2.1. These two procedures provide very similar structures and a residual charge, which does not differ by more than 0.2%.

3. Simulation Methods

The isotherms of adsorption were computed using grand canonical molecular dynamic (GCMD) simulations combined with an explicit reservoir of gas.[39] We used the full insertion/deletion[40] trial move to model an open system. Additionally, by comparison with the fractional[41] particle insertion/deletion, we obtain the right frequency of insertion. Indeed, the fractional method allows for getting stable dynamics, whereas in the full approach, if the frequency of insertion is higher or the MD move is too low, an alteration of the dynamics is found. In contrast to the GCMC simulations, the kinetic energy is included in the partition function (eq 5). Hence, the GCMD method will allow us to model a dynamical description of the confinement and adsorption process.

$$Q_{\mu VT} = \frac{1}{h^{3N}N!}\int\int d\mathbf{r}^N\, d\mathbf{p}^N \exp(-(\beta[U(\mathbf{r}^N) + K(\mathbf{p}^N) - \mu N]) \tag{5}$$

In eq 5, U and K are the potential and kinetic energies respectively, μ is the chemical potential, $\mathbf{p}^N$ the momentum vector, $\mathbf{r}^N$ the positions, β is the reverse temperature ($1/(k_B T)$), where k_B is the constant of Boltzman, N the total number of molecules, and h is Planck's constant. The initial kinetic energy of the inserted molecules was calculated from the Maxwell−Botzmann distribution. The expression of the probability of acceptance of the deletion/insertion trial move is given in ref 41. We used a modified DL_POLY package[42] to compute the isotherms of adsorption using the grand canonical molecular dynamic (GCMD) simulations. We used the Ewald summation for the computation of electrostatic interactions, and the long-range corrections were applied from $r = 12$ Å. For GCMD, the full insertion/deletion trial move was attempted every 100 configurations to reach the mechanical and thermal equilibrium at $T = 300$ K. The simulations were performed using a time step of 0.002 ps over an acquisition phase of 2 ns. The equilibration time was fixed to 5 ns to allow stabilization of the amount adsorbed, energy, temperature, and pressure. Here, we study a larger size of pore rather than the long time properties, given that the size effect in the confinement is problematic. A reduction of the number of interactions to be calculated is one straightforward strategy to access longer time scale than those usual atomistic models. We believe that this second strategy can equally illustrate the capability of the approach. It has been preferred because it allows one to investigate another pore diameter which was not reachable to an atomistic description in a reasonable time. Changing the pore size from micro to mesoporous diameters is indeed a crucial issue in exploring the physics of confinement. Size effects have been widely investigated experimentally for a variety of pore sizes, including diameters as large as some tens of nanometers (with SBA-15 silicates for instance) where departure from the bulk is initiated. This is a range of pore sizes where improvements in molecular simulation are needed. The AA model of MCM-41 for $D = 25$ Å and 50 Å implies 2012 and 11384 atoms, respectively. The same porous systems described by the CG model require 1322 and 7480 sites, respectively. One consequence of the reduction

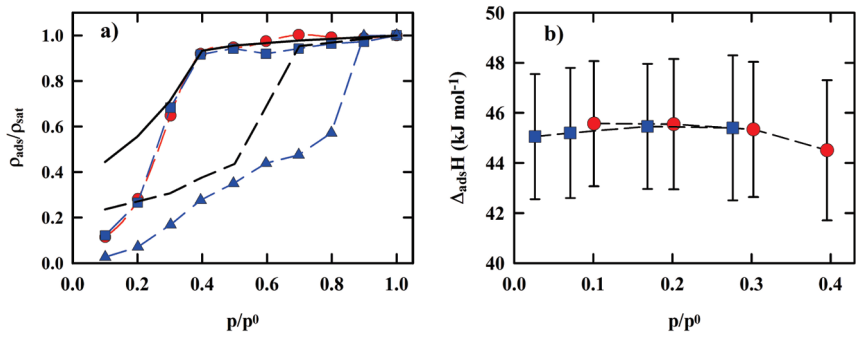

Figure 3. Isotherm (a) and enthalpy (b) of adsorption of methanol in MCM-41 for a pore diameter (D) of 24 Å for AA (●) and CG/AA force fields (■). In figure a, black dashed and solid lines are the experimental data for $D = 24$ Å and $D = 50$ Å, respectively. ▲ corresponds to the computed isotherm for $D = 50$ Å using the CG/AA model. ρ is the number of molecules per unit of volume.

in the number of interaction sites induced by coarse-graining is an increase in computation time (by a factor of about 1.5 in the present cases). Figure 1c shows obviously the increase in time obtained with the CG/AA model in relation to the AA description. Molecular dynamics were run on an Intel Core 2 quad core 2.66 GHz CPU gigascale workstation. From parallelized molecular dynamics simulations, the time gained is very impressive. However, from Monte Carlo simulations, the computational time gain is less convincing, and then the CG description and the rigid considerations can decrease it. At saturation, the CPU times of sequential Monte Carlo simulations for CG/AA and AA model descriptions are 61.1 and 30.2 h, respectively. This gain can be increased from a higher coarse-graining level. Combination of the CG/AA description and parallel MD simulations is an open way to the possible extension of simulation studies to larger time and length scales. Petascale architectures are a very promising technology for exploring the large-sized systems. Indeed, the MD simulations are 1000 faster, which allows for reaching the microsecond time scale. We think that the combination of the petascale machines and the CG description will allow the exploration of very large length and time scales. Then, it is important to develop the methodologies as presented in this work to decrease the complexity of the studied systems. Indeed, the size and the complexity of these nearly increase with the power of the computer. Combination of the CG/AA model with petascale architectures will improve the exploring and understanding of the physics properties under confinement.

The coarse-graining procedure keeps the surface roughness and mesostructure (related to SANS) unchanged with respect to the initial AA model. Some better insights into the microstructure and surface roughness could be beneficial to the description of some materials of current interest, such as porous silicon or SBA-15. In these cases, quenched disorder induced by large surface roughness as well as microporosity inside the wall have been discussed mainly from the experimental side and in a limited number of promising simulation works. These studies would go beyond the simple case of MCM-41 addressed here but are of major interest.

4. Results and Discussion

4.1. Highly Hydrated MCM-41. We report in Figure 2a and b the reduced enthalpy of adsorption $\Delta_r H_{ads}$[43](eq A1 of the Appendix) and the adsorbed amount, n_{ads}, as function of the reduced pressure for the AA and CG/AA force fields.

We obtain a perfect agreement between the two models for a pore diameter of $D = 2.4$ nm for the two physical properties. This validates the coarse-graining method used to describe the mesoscopic interactions between the porous framework and the adsorbate. This allows us to take advantage of the gain in computation speed provided by the coarse-grained description. For instance, we have performed CG/AA simulations of a larger pore size ($D = 5$ nm). We observe a significant shift of the pressure of capillary condensation for the two pore sizes from about $P = 0.3$ to $P = 0.8$. This can be attributed to the different density of silanol at the inner surface. This pore size effect on the adsorption isotherm is in qualitative agreement with experimental results obtained for the same pore size and shown as filled symbols in Figure 2a.[44] However the agreement between simulations and experiments is not fully quantitative, especially the capillary condensation which occurs around $P = 0.6$ for the largest pore in the experimental case. Although, this would mean that the AA interaction parameters could probably be improved, it does not affect our conclusions about the validity of the coarse-graining procedure. As a hint for future studies, it is most probable that the adsorption properties are sensitive to small variations of the nature of the hydrophilic surfaces of the MCM-41 used in the different experiments—in terms of silanol density, for instance. This is a crucial parameter that can be tuned in the simulation models to monitor its influence on the physics of confined materials. A critical check of the coarse-grained model with respect to interfacial interaction and liquid structure is provided by the number of hydrogen bonds and the radial density profiles shown in Figure 3a and b, respectively.

Hydrogen bonds between methanol and silanol groups (Me−HO···HO−Si and Me−OH···(OH)Si) have been defined according to commonly used geometrical criteria.[45] They have been calculated as a function of pressure and presented in Figure 4a after normalization to one methanol or one silanol. At the lowest pressure, about one H bond

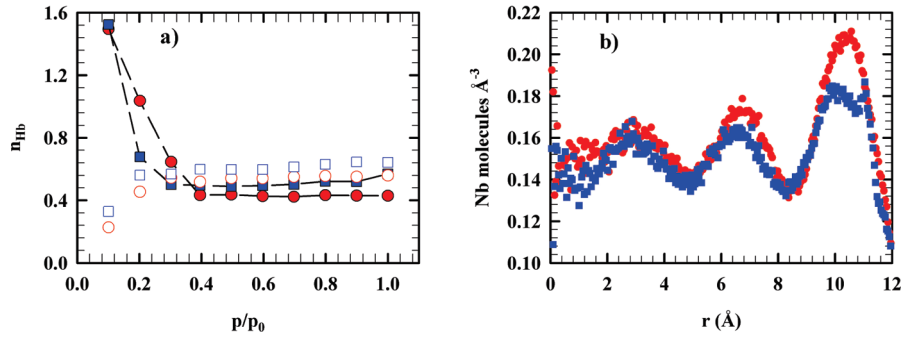

Figure 4. (a) Number of hydrogen bonds between the hydrogen atom of methanol and oxygen atom of the silanol located at the internal surface (and the oxygen atom of methanol and the hydrogen atom of silanol) per silanol (full symbols) and per methanol (empty symbols). The circle and square symbols represent the AA and CG/AA models, respectively, at $p/p_0 = 1$. (b) Radial distributions of methanol in the pore ($D = 24$ Å) using two models: AA (●) and CG/AA (■).

per methanol is formed, which means that in the regime of low coverage, methanol molecules are essentially adsorbed on silanol sites. In the gas phase, the competition between methanol/methanol and silanol/methanol interactions mostly favors surface adsorption.

This average number decreases on increasing the loading, since multiple layers are formed, which leads to an increasing number of methanol molecules far from the interface and the occurrence of more methanol−methanol interactions. In the dense liquid phase, the competition between the different types of interactions is balanced, and they equally contribute to the enthalpy of the system. At complete loading (264 molecules), the number of H bonds per silanol saturates to only about 0.6. This incomplete saturation of surface H-bonded sites means that steric hindrance near the pore wall probably prevents surface silanols from forming more H bonds. These features are equally observed for the AA and CG/AA models, suggesting that the interfacial fluid/framework interactions are correctly described. We obtain the same concordance for the radial profiles of methanol in the pore (Figure 4b). The CG model nicely captures the details of the layering organization at ambient pressure as well as the structural organization at the interface, which are key features of the confinement effect on fluid properties.[31] The difference in radial density between the AA and CG/AA models near the walls is due to the difference in the adsorbed amount.

As for dynamic properties, we provide in Figure 4a the 3D average translational diffusion coefficient D_t. It is obtained from the time evolution of the isotropic mean-square displacement (MSD) of the molecular center-of-mass according to eq 6. In this equation, N_0 is the number of the origin time (t_0), t is the MD time, r the vector position of the centre of mass (com) and N the number of the particles.

Same values of D_t are obtained within the statistical uncertainties for the two models, which gives support to the coarse-graining procedure with respect to the dynamical behavior too. With increasing pressure, the value of D_t decreases systematically, which can be related to the increase of the average density of the confined phase during filling and the collapse of the free liquid−gas interface.

$$D_t = \lim_{t\to\infty} \frac{\langle \sum_{t_0}^{N_0} \sum_{i=1}^{N} |r_{com,i}(t + t_0) - r_{com,i}(t)|^2 \rangle}{6NN_0t} \quad (6)$$

In order to get better insight into the translational dynamics, we compare in Figure 4b the MSD along the three directions of space, x, y, and z, and their isotropic average for the two models at complete filling, $p/p_0 = 1$.

A crossover is observed around $t = 100$ ps in the time variation of the MSD measured along the z direction of the pore axis (Figure 5b). It corresponds to a change of the translation motion from subdiffusive at short times to fully diffusive at longer times (i.e., MSD(t) $\sim t$ [blue line]), which is a typical feature of the dynamics of dense liquids. At variance in the two directions perpendicular to the pore axis (x and y), the short-time subdiffusive regime is not followed by a diffusive regime. On the contrary, the MSD bends and reaches a plateau value for times longer than 1 ns. This anisotropy in the transport reflects the effects of the unidirectional spatial confinement, which primarily constrains molecule motions in the x and y directions. Experimental and numerical signatures of similar low-dimensional diffusion have been reported in the literature for different sorts of confined materials.[46−48] Again, the details of these dynamical features are well reproduced by the CG/AA model.

Finally, we checked the transferability of the model, which is one crucial criterion for the prediction of thermodynamic properties. We computed the isotherm of adsorption of water in silica for a pore size $D = 2.4$ nm using the TIP4P2005 model for water[48] and the AA and CG/AA force fields discussed previously for the mesoporous silicate. Figure 6 shows excellent agreement between the adsorbed quantities obtained for the two different models.

Furthermore, a comparable agreement is obtained for the enthalpy of adsorption[43] at low pressures, which is 45 ± 1.1 kJ mol^{-1} for AA and 46 ± 0.9 kJ mol^{-1} for CG/AA. This successful test with respect to the adsorption isotherm and an energetic quantity shows the high transferability of the CG/AA force field to some other molecular adsorbates.

4.2. Weakly Hydrated MCM-41. Figure 7a shows the isotherms of adsorption of AA and CG/AA force fields of the weakly hydrated porous silicates. It exhibits a good

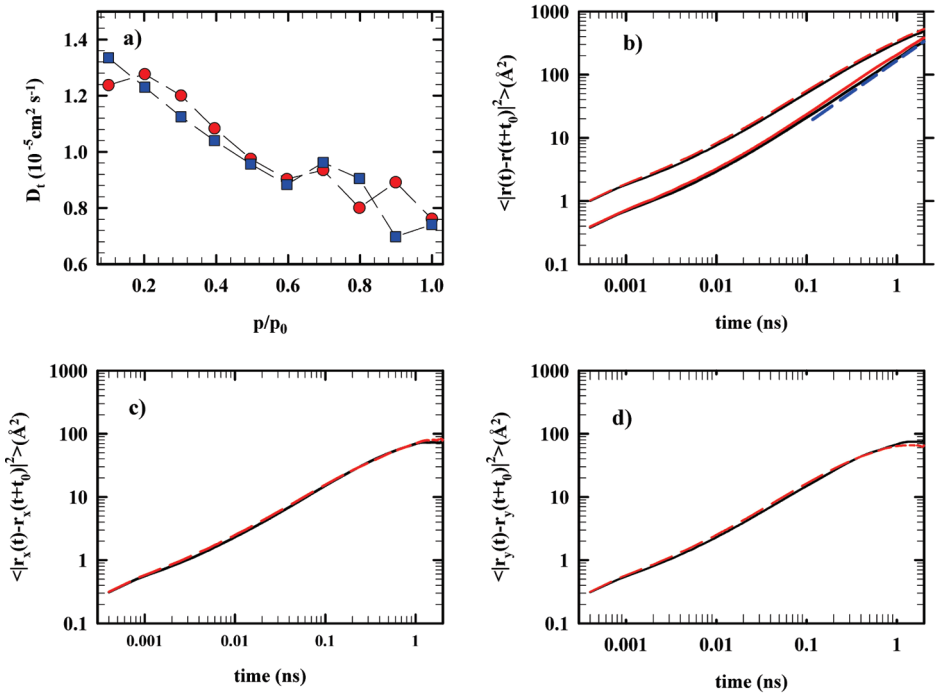

Figure 5. (a) Translational diffusion of methanol using two models: AA (●) and CG/AA (■) as function of the reduced pressure. Mean square displacement (MSD) of methanol into the pore ($D = 24$ Å) according to the x (c), y (d), and z and total components (b). The red dashed line represents the CG/AA model, while the black solid line corresponds to the AA model. Parts b, c, and d are represented in logarithmic scale. In part b, we reported the curve (blue dashed line) of $y = Dt$ as a guide for the eye.

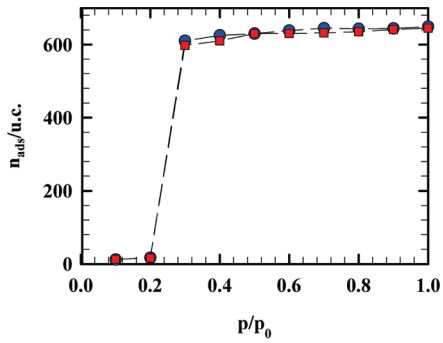

Figure 6. Isotherm of adsorption of water in a pore of diameter $D = 24$ Å, using two models: AA (●) and CG/AA (■).

accordance between the two models, which further validates our multiscale optimization method. Figure 7b provides a comparison between the isotherms of adsorption of methanol in WH and HH MCM-41, where direct effects of the hydrophilic character of the surface on the adsorption properties can be observed. We have considered three different regions of the adsorption curves, labeled A, B, and C in Figure 7a. In region A, which corresponds to low pressure, we have a higher adsorbed amount for WH MCM-41 than for HH. This trend is inversed in region B, since the capillary filling is shifted to higher pressure for the WH material. Finally, in region C, a slightly higher adsorbed quantity is reached for the WH form at complete loading.

A greater adsorbed amount in regions A and C, for the WH material with respect to the HH, can be related to the greater accessible surface and porous volume of the former material, respectively. The adsorption mechanism in region A mostly corresponds to the pore surface coverage by methanol. The adsorbed amount is therefore sensitive to the accessible surface (S_{acc}), which has become larger for the WH material after removal of a part of the surface silanol groups. To get a more quantitative depiction, we calculate the accessible surface area (usually denoted ASA in the literature), which corresponds to the area traced out by the center of a probe molecule as the probe is rolled across the surface of the framework atoms. In practice, the accessible surface area is obtained from a simple Monte Carlo integration where the probe sphere is randomly inserted around the surface of each framework atom in turn and tested for overlap.[38] The fraction of probes that do not overlap with other framework atoms is used to calculate the accessible surface area. The probe should be chosen to correspond to the size of the adsorbate of interest, i.e., 3.9 Å for the methanol molecule. According to this procedure, we obtain S_{acc}(HH) = 2840.03 Å^2 and S_{acc}(LH) = 3078.09 Å^2, which is consistent with the different adsorbed amount at low pressure controlled by the state of the surface. For similar reasons, the slightly larger adsorbed amount at complete filling (region C) for the WH materials can be related to a larger accessible volume (linked to a larger S_{acc}) induced by silanol group removal during surface dehydration.

The inversion in region B is related to a shift to higher pressure of the capillary condensation for the WH material. The pressure of capillary condensation, which corresponds to a rather steep increase of the adsorbed amount at intermediate pressure, is closely related to the value of the fluid−pore interaction as well as the pore size. A weaker fluid−pore interaction is expected for methanol when the surface hydrophobicity is tuned from high (for the HH MCM-41) to moderate (for the WH MCM-41). On the microscopic

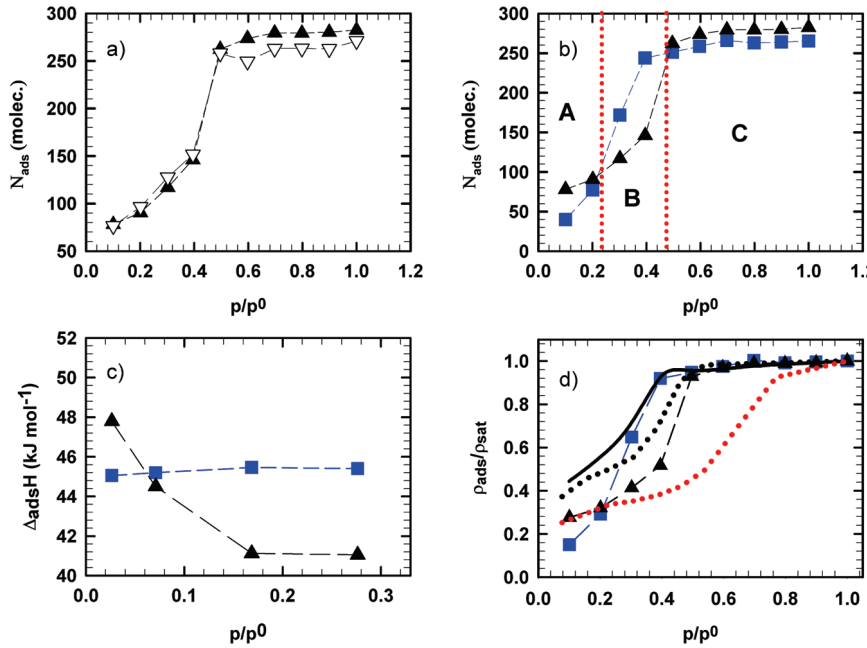

Figure 7. (a) Isotherm of the adsorption of methanol in a pore of the weakly hydrated porous silicates with diameter $D = 24$ Å, using two models: AA (▲) and CG/AA (▽). Isotherm (b) and enthalpy (c) of the adsorption of methanol in a pore of diameter $D = 24$ Å using the AA force field for WH (▲) and HH (■) MCM-41. (d) Isotherm of the adsorption of methanol in a pore of diameter $D = 24$ Å using the AA force field for WH (▲) and HH (■) MCM-41. Experimental isotherms for $D = 24.1$[44] Å (solid line), $D = 21$ Å (dotted line), and $D = 28$ Å (red dotted line) taken from ref 50.

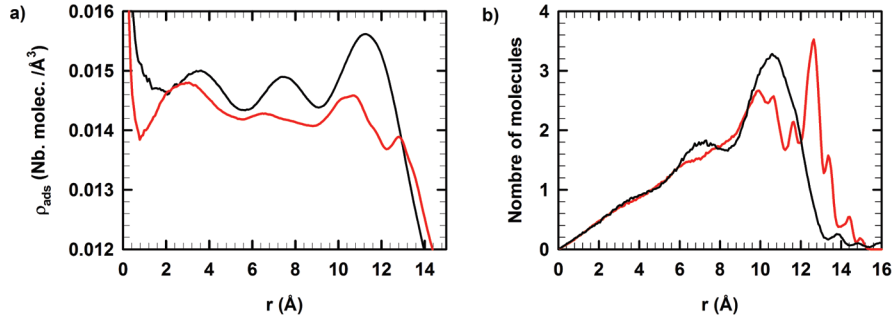

Figure 8. (a) Radial density of the methanol for HH (black line) and WH (red line) MCM-41. (b) Number of methanol molecules as a function of the distance from the center of the pore.

scale, this phenomenon can be related to the lower tendency of methanol to form an interfacial network of hydrogen bonds with the WH silicate. This interpretation is confirmed by the calculation of the number of hydrogen bonds by silanols groups in the two forms (∼0.4 in HH and ∼0.2 in WH at complete loading). This behavior is also reflected by the variation of the adsorption enthalpy (Figure 6c) where we observe a similar crossover from regions A and B for the two types of porous materials. Figure 6d shows a fair agreement between our simulation results for the HH form of MCM-41 and the experimental isotherm of adsorption from Carrot et al. for $D = 24$ Å[33] while the WH isotherm is shifted to higher pressure. It would suggest that the highly hydrated form considered in this case provides a more realistic description of the experimental sample. However, if we consider the more recent work on materials where a low silanol density was reported (2−3 OH/nm^2), it appears that our simulated adsorption curve for the WH MCM-41 with diameter $D = 24$ Å lies nicely between the two experimental curves obtained for adjacent values of diameter $D = 21$ and 28 Å.[49,50] This can be considered as a valuable test of the validity of our derivation of a CG/AA force field for MCM-41.

Finally, we compare the radial density profile of methanol for WH and HH MCM-41 at saturation in order to analyze the effect of silanol density on the layered structure in the confined liquid. As discussed in the previous section, methanol confined in the HH form exhibits a strongly layered structure, as shown in Figure 8a. This radial structuring of the fluid is weaker in the WH porous silicate: the amplitude of the modulation of density is smaller, and the peaks are broader. In addition, the density profile of the contact layer ($r > 8$ Å) exhibits two maxima. Layering is induced by the enhancement of methanol order from the solid surface that propagates toward the inner pore. This effect is expected to be smaller for the WH materials, because it induces a smaller number of interfacial H bonds between methanol and silanol groups. In addition, the WH surface presents sites with different hydrophilic character, which is at variance with the HH surface that is smooth and uniformly covered by silanols.

In the WH matrix, interfacial molecules can therefore feel a broader variety of local environments. It can induce different types of preferred configurations for the molecules located at the surface, as the shape of the density profile within the contact layer would suggest. This phenomenon further weakens the surface ordering effect.

5. Conclusion

Molecular simulations can provide unique contributions to a better understanding of the mesoporous confinement effect on fluid properties. They have been constantly improved by appropriate methodological developments.

Indeed, the physics of confined materials generally requires extending the investigation to long length and time scales. This can introduce strong limitations to the capability of all atoms descriptions, which are very time-demanding. On the other hand, full mesoscopic approaches are deficient in a sufficient microscopic account of the solid/fluid interfacial interactions.

For that purpose, we developed a general and multiscale procedure to design a hybrid coarse grained/all atom force field that gathers the benefits of both approaches: it includes an atomistic description of the inner pore surface, including a realistic account of silanols and a coarse-grained description of the overall porous framework. We presented a derivation method based on the optimization of the CG parameters with respect to macroscopic properties, i.e., the adsorbed amount and the enthalpy of adsorption calculated by AA and CG simulations. We have fully validated our approach in the case of methanol adsorbed in a MCM-41 material. This coarse-graining method is fast and versatile. We have shown a good reproduction of both static and dynamical properties, in terms of adsorbed quantity, isosteric heat of adsorption, interfacial structure, and translation coefficient. Besides, we have shown that GC/AA provides promising openings for simulation of much larger systems, as illustrated with a pore of diameter 5 nm and is fully transferable to other adsorbates, such as water. We have also shown that the GC/AA can address the currently debated question of the effect of the hydrophilic character of the porous materials on the adsorption properties and the liquid structure. Indeed, it fully accounts for the presence of surface silanol groups, the number of which can be tuned as shown in our comparative study for two MCM-41's with different hydration levels. Finally, this model represents a very interesting and powerful intermediate model between all microscopic and mesoscopic descriptions. This method can be easily transferred to the other porous materials with the specific sites of interactions such as metal organic framework (MOF), covalent organic framework, or polymer coordination from a higher degree of coarse graining. Additionally, other macroscopic properties can be used in the derivation process.

Appendix

The calculation of $(\partial\Delta_n H_{ads})/(\partial y)$ with $y = \varepsilon$ and σ implies a reminder of the definition of $\Delta_n H_{ads}$ (eq A1).

$$\Delta_r H_{ads} = \frac{\langle n_{ads} H\rangle - \langle n_{ads}\rangle\langle H\rangle}{\langle n_{ads}^2\rangle - \langle n_{ads}\rangle^2} \tag{A1}$$

In eq A1 n_{ads} is the amount adsorbed and H the total Hamiltonian of the system composed of potential and kinetic terms. For more clarity, we omitted the dependence with respect to **r** and **p** in the Halmitonian (H).The derivation with respect to y provides eq A2.

$$\frac{\partial\Delta_n H_{ads}}{\partial y} = \frac{1}{(\langle n^2\rangle - \langle n\rangle^2)}\left[\left(\frac{\partial(nH)}{\partial y} - \langle H\rangle\frac{\partial\langle H\rangle}{\partial y} - \langle n\rangle\frac{\partial\langle H\rangle}{\partial y}\right)(\langle n^2\rangle - \langle n\rangle^2) - \left(\langle nH\rangle - \langle n\rangle\langle H\rangle\left(\frac{\partial(n^2)}{\partial y} - 2\langle n\rangle\frac{\partial\langle n\rangle}{\partial y}\right)\right)\right] \tag{A2}$$

For more clarity we omit the subscript ads. The terms $(\partial\langle nH\rangle)/(\partial y)$, $n(\partial\langle H\rangle)/(\partial y)$, $(\partial\langle n\rangle)/(\partial y)$, $(\partial\langle n^2\rangle)/(\partial y)$, and $(\partial\langle H\rangle)/(\partial y)$ have been determined by following relations while $\langle(\partial H)/(\partial y)\rangle$ is evaluated by a first-order finite difference.

$$\frac{\partial\langle nH\rangle}{\partial y} = \left\langle n\frac{\partial H}{\partial y}\right\rangle - \beta\left(\left\langle (nH)\frac{\partial H}{\partial y}\right\rangle - \langle nH\rangle\left\langle\frac{\partial H}{\partial y}\right\rangle\right) \tag{A3}$$

$$\frac{\partial\langle n\rangle}{\partial y} = -\beta\left(\left\langle n\frac{\partial H}{\partial y}\right\rangle - \langle n\rangle\left\langle\frac{\partial H}{\partial y}\right\rangle\right) \tag{A4}$$

$$\frac{\partial\langle n^2\rangle}{\partial y} = -\beta\left(\left\langle (n^2)\frac{\partial H}{\partial y}\right\rangle - \langle n^2\rangle\left\langle\frac{\partial H}{\partial y}\right\rangle\right) \tag{A5}$$

$$\frac{\partial\langle H\rangle}{\partial y} = -\beta\left(\left\langle (H)\frac{\partial H}{\partial y}\right\rangle - \langle H\rangle\left\langle\frac{\partial H}{\partial y}\right\rangle\right) \tag{A6}$$

References

(1) Gelb, L. D.; Gubbins, K. E.; Radhakrishnan, R.; Sliwinska-Bartkowiak, M. *Rep. Prog. Phys.* **1999**, *62*, 1573.

(2) Christenson, H. K. *J. Phys Cond. Mat.* **2001**, *13*, R95–R133.

(3) Alcoutlabi, M.; McKenna, G. B. *J. Phys.: Cond. Matter* **2005**, *17*, R461.

(4) Alba-Simionesco, C.; Coasne, B.; Dosseh, G.; Dudziak, G.; Gubbins, K. E.; Radhakrishnan, R.; Sliwinska-Bartkowiak, M. *J. Phys.: Condens. Matter* **2006**, *18*, R15.

(5) Klein, J.; Kumacheva, E. *Science* **1995**, *269*, 816.

(6) Granick, S. *Science* **1991**, *253*, 1374.

(7) Bellini, T.; Radzihovsky, L.; Toner, J.; Clark, N. A. *Science* **2001**, *294*, 1074.

(8) Coasne, B.; Jain, S. K.; Gubbins, K. *Phys. Rev. Lett.* **2006**, *97*, 105702.

(9) Guégan, R.; Morineau, D.; Lefort, R.; Moréac, A.; Béziel, W.; Guendouz, M.; Zanotti, J.-M.; Frick, B. *J. Chem. Phys.* **2007**, *126*, 1064902.

(10) Lefort, R.; Morineau, D.; Guégan, R.; Guendouz, M.; Zanotti, J.-M.; Frick, B. *Phys. Rev. E* **2008**, *78*, 040701(R).

(11) Coasne, B.; Hung, F. R.; Pellenq, R. J.-M.; Siperstein, F. R.; Gubbins, K. E. *Langmuir* **2006**, *22*, 194.

(12) Puibasset, J.; Pellenq, R. J.-M. *J. Chem. Phys.* **2005**, *122*, 094704.

(13) Coasne, B.; Renzo, F. D.; Galarneau, A.; Pellenq, R. J.-M. *Langmuir* **2008**, *24*, 7285.

(14) Guégan, R.; Morineau, D.; Loverdo, C.; Béziel, W. *Phys. Rev. E.* **2006**, *73*, 011707.

(15) Kityk, A. V.; Wolff, M.; Knorr, K.; Morineau, D.; Lefort, R.; Huber, P. *Phys. Rev. Lett.* **2008**, *101*, 187801.

(16) Neri, M.; Anselmi, C.; Cascella, M.; Maritan, A.; Carloni, P. *Phys. Rev. Lett.* **2005**, *95*, 218102.

(17) Hoogerbrugge, P. J.; Koelman, J. *Eur. Phys. Lett.* **1992**, *19*, 155.

(18) Flekkøy, E. G.; Coveney, P. V. *Phys. Rev. Lett.* **1999**, (83), 1775.

(19) Chen, N.-Y.; Su, Z.-Y.; Mou, C.-Y. *Phys. Rev. Lett.* **2006**, *96*, 078103.

(20) Detcheverry, F. A.; Pike, D. Q.; Nealey, P. F.; Müller, M.; Pablo, J. J. d. *Phys. Rev. Lett.* **2009**, *102*, 197801.

(21) Dupuis, L. M.; Tadmor, E. B.; Miller, R. E.; Phillips, R. *Phys. Rev. Lett.* **2005**, *95*, 060202.

(22) Fabritiis, G. D.; Delgado-Buscalioni, R.; Coveney, P. V. *Phys. Rev. Lett.* **2006**, *97*, 134501.

(23) Dubbeldam, D.; Calero, S.; Vlugt, T. J. H.; Krishna, R.; Maesen, T. L. M.; Beerdsen, E.; Smith, B. *Phys. Rev. Lett.* **2004**, *93*, 088302.

(24) Ashbaugh, H. S.; Patel, H. A.; Kumar, S. K.; Garde, S. *J. Chem. Phys.* **2005**, *122* (10), 104908.

(25) Elezgaray, J.; Laguerre, M. A. *Comput. Phys. Commun.* **2006**, *175* (4), 264.

(26) Lyubatsev, A. P. *Eur. Biophys. J. Biosphys. Lett.* **2005**, *35* (1), 5361.

(27) Ivzvekov, S.; Voth, G. A. *J. Phys. Chem. B* **2005**, *109* (7), 2469.

(28) Das, A. C.; Andersen, H. *J. Chem. Phys.* **2009**, *131*, 034102.

(29) Gupta, N. M.; Kumar, D.; Kamble, V. S. S.; Mitra; Mukhopadhyay, R.; Kartha, V. B. *J. Phys. Chem. B* **2006**, *110*, 4815.

(30) Takahara, S.; Kittaka, S.; Mori, T. Y.; Kuroda; Takamuku, T.; Yamaguchi, T. *J. Phys. Chem. C* **2008**, *112*, 14385.

(31) Guégan, R.; Morineau, D.; Alba-Simionesco, C. *Chem. Phys.* **2005**, *317*, 236.

(32) Morineau, D.; Guégan, R.; Xia, Y.; Alba-Simionesco, C. *J. Chem. Phys.* **2004**, *121*, 1466.

(33) Ribeiro Carrot, M. M. L.; Candeias, A. J. E.; Carrot, P. J. M.; Ravikovitch, P. I.; Neimark, A. V. *Microporous Mesoporous Mater.* **2001**, *47*, 323–337.

(34) Vink, R. L. C.; Barkema, G. T. *Phys. Rev. B* **2003**, *67*, 245201.

(35) Bródka, A.; Zerda, T. W. *J. Chem. Phys.* **1996**, *104*, 6319.

(36) Chen, B.; Potoff, J. J.; Siepmann, J. I. *J. Phys. Chem. B* **2001**, *105*, 2569.

(37) Bourasseau, E.; Haboudou, M.; Boutin, A.; Fuchs, A. H.; Ungerer, P. *J. Chem. Phys.* **2003**, *118*, 3020.

(38) Allen, M. P.; Tildesley, D. J. *Computer Simulation of Liquids*; Oxford University Press: New York, 1987.

(39) Chempath, S.; Clark, L.; Snurr, R. *J. Chem. Phys.* **2003**, *118*, 7635.

(40) Lupkowski, M.; Swol, F. v. *J. Chem. Phys.* **1991**, *95*, 1995.

(41) Boinepalli, S.; Attard, P. *J. Chem. Phys.* **2003**, *119*, 12769.

(42) Forester, T. R.; Smith, W. *DLPOLY CCP5 Program Library*; Daresbury Lab.: Cheshire, U. K., 1994.

(43) Nicholson, D.; Parsonage, N. G. *Computer Simulation and the Statistical Mechanics of Adsorption*; Academic Press: London, 1982.

(44) Ghoufi, A.; Morel, J. P.; Desrosiers, N. M.; Malfreyt, P. *J. Phys. Chem. B* **2005**, *109*, 23579.

(45) Busselez, R.; Lefort, R.; Ji, Q.; Affouard, F.; Morineau, D. *Phys. Chem. Chem. Phys.* **2009**, *11*, 11127.

(46) Malikova, N.; S.; Longeville, S.; Zanotti, J.-M.; Dubois, E.; Marry, V.; Turq, P.; Ollivier, J. *Phys. Rev. Lett.* **2008**, *101*, 265901.

(47) Scheidler, P.; Kob, W.; Binder, K. *J. Phys. Chem. B* **2004**, *108*, 6673.

(48) Vega, C.; de Miguel, E. *J. Chem. Phys.* **2007**, *126*, 154707.

(49) Takamuku, T.; Maruyama, H.; Kittaka, S.; Takahara, S.; Yamaguchi, T. *J. Phys. Chem. B* **2005**, *109*, 892.

(50) Yamagushi, T.; Yoshida, K.; Smirnov, P.; Takamuku, T.; Kittaba, S.; Takahara, S.; Kuroda, Y.; Bellissent-Funel, M. C. *Eur. Phys. J.* **2007**, *141*, 19–27.

CT100169R